Wave Propagation in a Fluid Filled Rubber Tube: Theoretical and Experimental Results for Korteweg's Wave

François Gautier, Joël Gilbert, Jean-Pierre Dalmont, Ruben Pico

WAVE PROPAGATION IN A FLUID FILLED RUBBER TUBE: THEORETICAL AND EXPERIMENTAL RESULTS FOR KORTEWEG'S WAVE

F. Gautier [1], J. Gilbert [1], J.-P. Dalmont [1], R. Picó Vila [2]

[1] Laboratoire d'Acoustique de l'Université du Maine, UMR CNRS 6613, Av. O. Messiaen, 72085 Le Mans cedex 9, France

Email:[**Francois.Gautier, Joel.Gilbert, Jean-Pierre.Dalmont]@univ-lemans.fr**

[2] Dept. Física Aplicada, Esc. Politécnica Superior de Gandia, Universidad Politécnica de Valencia, Carretera Nazaret-Oliva s/n, 46700 Valencia, Spain

Email : **rpico@fis.upv.es**

Total number of pages: 42

Total number of figures: 14

Total number of tables: 1

Short title: Wave propagation in a fluid-filled cylindrical membrane

Professional address of the corresponding author:

Francois Gautier

Laboratoire d'Acoustique de l'Université du Maine, UMR CNRS 6613, Av. O. Messiaen, 72085 Le Mans cedex 9, France

e-mail: **Francois.Gautier@univ-lemans.fr**

Abstract:

In this paper, the interaction between the wall vibrations of a stretched elastic cylindrical membrane and the inner acoustic field is considered under plane wave approximation. Three waves exist at low frequencies for this coupled system. The first of these, called Korteweg's wave, propagates mainly within the fluid and corresponds to the acoustic plane wave which is closely coupled to the wall vibrations. The two other waves mostly propagate within the structure and correspond to coupled longitudinal/flexural motions: one corresponds to predominant longitudinal motions in the membrane and the other exists only when tension is applied to the membrane and is similar to a string bending wave. A model for the dispersion curves is presented and is experimentally validated. In particular, the model and experiments reveal that three frequency ranges exist for which the propagation of the Korteweg's wave is subsonic, evanescent and supersonic. The experimental validation is achieved using the acoustic impedance measurements for a stretched rubber membrane. Assuming that the vibratory and acoustic fields are dominated by one wave, the latter are described by using only one dispersive wave, in this case, of equivalent wave speed. The input acoustic impedance curve can be fitted using this expression which only requires one equivalent wave.

1. Introduction

The vibroacoustics of cylindrical ducts have been extensively studied throughout the relevant literature since numerous applications in mechanical engineering involve fluid-filled pipes with yielding walls. Within the framework of thin shell theories as described in [1], wave propagation in fluid-filled cylindrical shells has been investigated in [2], [3], [4] and the branches of the dispersion curves depending on the modal circumferential indices have been presented. In the light fluid approximation, the dispersion curves of the fluid-filled shell can be interpreted as the juxtaposition of the *in vacuo* shell dispersion branches and the acoustic dispersion branches of the rigid walled tube. For heavy fluid, the fluid loading term is of importance such that it is not possible to interpret the dispersion diagram in a similar manner with this juxtaposition. In this case, the modes of the coupled system differ greatly from the acoustical modes of the rigid duct and the structural modes of the *in vacuo* shell.

A strong interaction between fluid and structure also occurs when the tube wall is very flexible. This is the case for cylindrical rubber membranes submitted to a static tension which are studied in this paper: attention is focused on fluid-structure interaction between the plane acoustic wave and the membrane breathing motions. A study of this configuration is carried out using theoretical and experimental approaches and is structured as follows : following a short bibliographical review (Section 2.1), a vibroacoustic model of a membrane submitted to a static preload is described in Section 2.2. A dispersion equation is derived (Section 2.3) and free wave expansion is used to compute the acoustic input impedance of the tube (Section 2.4). In Section 3, measurements of the input impedance are presented and an equivalent speed for the propagating waves within the system is obtained. Finally, the limitations of the model and the main results are summarized in the conclusion.

2. Vibroacoustic model of a fluid filled rubber tube

2.1 Korteweg's model : Bibliographical review

Analytical vibroacoustic models of waveguides with yielding walls are based on assumptions related to the following three descriptions; that of the inner acoustic pressure,

the wall motion and the fluid-structure interaction. The description of the acoustic pressure field can be achieved in the most general manner using multimodal expansion as presented in [2]. Descriptions of the wall motion can be achieved using 3D elasticity [5], Donnell's thin shell theory [2], Flugge-Timoshenko's theory [4], membrane theory [6], or a local wall admittance model [7]. A description of the fluid-structure interaction is generally based on a continuity relation of the normal velocity. However, an acoustic treatment on the walls can also be modeled using appropriate wall impedance.

When considering the axisymmetric motions for the shell, and plane acoustic motion for the inner fluid, it can be shown that the dispersion equation for the fluid-filled shell has five pairs of roots $\pm\lambda$ for each frequency, associated with five waves travelling in both directions. The corresponding waves of the coupled system are the quasi-plane acoustic wave (Korteweg's wave), the speed of which is disturbed by wall vibration, and four waves which mainly propagate within the structure : the torsional shell wave is completely uncoupled from the fluid motion. A quasi-longitudinal wave propagates mainly within the shell. Two other waves are longitudinal/flexural waves which mostly propagate inside the shell and which are evanescent below the shell's ring frequency. A discussion regarding dispersion curves for a wide range of parameters is given in detail in [2] for breathing modes (corresponding to the circumferential order $m=0$) and for bending modes ($m=1$).

The first of these five waves, corresponding to the quasi plane acoustic wave can be described without using shell theory for the description of the wall : in a simplified way, coupling can be described by a wall admittance implying that the reaction of the wall is local. In this model, the forces applied to an elementary fluid volume located between two cross sections of the duct very close to each other are related to the compressibility effect and the wall effect. This wall effect is known as the distensibility effect (see [8], [9]). The speed of the acoustic plane wave depends on both the compressibility and distensibility effects. The acoustic plane wave becomes strongly dispersive : subsonic, evanescent and supersonic frequency ranges can be distinguished. The frequency range in which the wave is evanescent corresponds to a stop band. This model was first presented by [10] during the 19th Century, and this wave type is called Korteweg's wave or Moens-Korteweg's wave. It corresponds to a simplified model giving a satisfactorily low frequency approximation of the first of the 5 waves listed above. In the literature, this model has been presented in several reference books [9], [7], [8], [11] and, it has been independently re-developed : Korteweg´s name does not systematically appear in the studies cited in the next paragraph although the model is used. In

the following section, several applications for which this model has been derived and applied are reviewed.

Korteweg's model has been applied to biomechanics, in particular to provide a description for the propagation of waves in airways and blood vessels. For medical applications, a non-invasive technique called AAAR (airway area by acoustic reflection, [12], [13]) has been developed to determine the internal bore of the airway. An acoustic pulse is generated at the opening of the patient's mouth and the acoustic reflection coming from the airway is measured. A model of wave propagation in the vibrating duct is required in order to determine the profile of the cross section from the echo measurement using an inverse method. The airway wall vibrations are one of the most important limitations of this technique (see [14]). The local reaction assumption, on which Korteweg's wave model is based, is used to describe the wall fluid interaction using a limited number of parameters. A similar model for the vocal tract is also required for applications to speech synthesis and analysis [13], [15].

Another application of Korteweg's wave is related to wave propagation in blood vessels. In this case, the distensibility of the tube is of far greater importance than the compressibility of the fluid, with the result that the fluid may be regarded as incompressible [8]. For the purpose of modeling wave propagation in blood vessels, a more comprehensive model takes into account the non-linear behaviour of the vessel wall, its internal damping and the influence of the viscosity of the fluid [16].

Wind instruments are other types of wave guides with yielding walls. The influence of the wall vibration on the musical sound emitted by a woodwind instrument, a brass instrument or an organ pipe is open to debate. Vibroacoustic models have been developed in order to quantify the wall vibration effect [17], [18]. A change of wave speed due to wall vibration can be approximated using Korteweg's model. A small frequency shift in the acoustic resonance frequencies can then be estimated [19]. Numerical computations for parameter values corresponding to organ pipes of circular, elliptic and square cross sections show that this frequency shift is too small to be perceptible. However, these conclusions must be carefully considered since the results are based on the local reaction assumption, which is not always satisfied because of the modal behaviour of the pipe.

Experimental validations of Korteweg's model, including measurements of the variation in the wave speed versus frequency, are in short supply throughout the literature. Phase velocity can be determined from the distance between crests where standing waves are

observable. For applications to physiology, such measurements are given in [20] for a rubber tube and an excised canine trachea and by [21] for a rubber tube.

The local reaction hypothesis is not always satisfied. The most simple duct in which this is the case is a rubber membrane [6]. In this case, two waves exist : a Korteweg's wave which propagates mainly in the fluid and a longitudinal wave which propagates mainly in the membrane. Since both waves are present in the fluid and the structure, it can be said that the local reaction hypothesis is not valid here. The validity of the local reaction hypothesis is discussed in [22], [23]. Because of the presence of the stop band for Korteweg's wave, it has been highlighted that this property can be used to design an acoustic muffler [20]. In addition, the introduction of flexible segments in a piping system is a convenient passive technique which can be used to reduce structure-borne sound. Since such flexible segments also affect fluid-borne sound, any computation of the insertion loss or the transfer matrix of a pipe assembly should take this flexibility into account as in [24]. With the same objective, a model of pipe assembly has been developed using Kennard's thin shell theory of and using expansion over 'in vacuo' modes [25].

For practical reasons, the flexible tube has to be reinforced in many applications. The wave propagation of a pressurized tube stiffened by crossed wire is examined in [26], [27]. The influence of internal pressurization and axial membrane stress is considered. It is shown that major changes in the fluid dominated wave speed can be observed when the fluid loading term is increased.

2.2. Governing equations

In this section, a cylindrical pipe filled with a compressible fluid is studied. Attention is focused on the vibroacoustic coupling between the inner fluid and the pipe. The influence of the external fluid is ignored. The pipe is submitted to a static axial tension T. It has a length L, a radius a, a wall thickness h, and is assumed to be thin ($h/a<<1$). The co-ordinate system is given in Figure 1; x and z are the axial and radial co-ordinates, u and w are the membrane displacements in accordance with these directions. Assuming linear elasticity approximations, the equations governing axisymmetric vibrations of the membrane can be written as follows (see Appendix A for details) :

$$\begin{pmatrix} \dfrac{\partial^2}{\partial x^2} - \dfrac{\partial^2}{{c_L}^2 \partial t^2} & \dfrac{\nu}{a}\dfrac{\partial}{\partial x} \\ \dfrac{\nu}{a}\dfrac{\partial}{\partial x} & \dfrac{1-\nu^2}{E}\dfrac{T}{A}\dfrac{\partial^2}{\partial x^2} - \dfrac{1}{a^2} - \dfrac{\partial^2}{{c_L}^2 \partial t^2} \end{pmatrix} \begin{pmatrix} u \\ w \end{pmatrix} = \begin{pmatrix} 0 \\ -\dfrac{p}{\rho {c_L}^2 h} \end{pmatrix}, \tag{1}$$

where E, ρ and ν are the Young's modulus, the density, and the Poisson's ratio of the rubber material respectively. Since the material is supposed to be viscoelastic, the Young's modulus should be complex valued. The speed c_L of longitudinal waves inside the material is given by $c_L = \sqrt{E/\rho\left(1-\nu^2\right)}$. The acoustic pressure in the tube denoted by p and $A = 2\pi a h$ is the cross-section area of the membrane.

Assuming linear acoustic approximations and plane wave propagation, the acoustic pressure p inside the pipe satisfies the following inhomogeneous wave equation [28] :

$$\frac{\partial^2 p}{\partial x^2} - \frac{1}{c^2}\frac{\partial^2 p}{\partial t^2} = \frac{2\rho_0}{a}\frac{\partial^2 w}{\partial t^2}, \tag{2}$$

where c is the speed of sound in air, and ρ_0 the density of air. The right hand side of equation (2) corresponds to an acoustic source describing the wall vibration effect on the inner pressure field.

Equations (1) and (2) give a set of three linear second order differential coupled equations, as a function of the three variables u, w and p depending on space co-ordinate x and time t.

2.3. Dispersion curves

2.3.1 Dispersion equation

When looking for solutions for travelling waves with an harmonic excitation of angular frequency ω, the variables $u(x)$, $w(x)$ and $p(x)$ are assumed to be written as $u(x) = u_0 e^{j\lambda x}$, $w(x) = w_0 e^{j\lambda x}$ and $p(x) = p_0 e^{j\lambda x}$ with λ being the wavenumber. The time factor $e^{j\omega t}$ is implicit and $u(x)$, $w(x)$, $p(x)$ represent the complex amplitudes of the quantities. By

substituting the harmonic variables in equations (1) and (2), we obtain a set of three homogeneous equations :

$$\begin{pmatrix} -\lambda^2 + k^2 & 0 & \frac{2\rho_0}{a}\omega^2 \\ 0 & -\lambda^2 + k_L{}^2 & \frac{\nu}{a} j\lambda \\ \frac{1}{\rho c_L{}^2 h} & \frac{\nu}{a} j\lambda & -\frac{1-\nu^2}{E}\frac{T}{A}\lambda^2 - \frac{1}{a^2} + k_L{}^2 \end{pmatrix} \begin{pmatrix} p_0 \\ u_0 \\ w_0 \end{pmatrix} = \begin{pmatrix} 0 \\ 0 \\ 0 \end{pmatrix}, \qquad (3)$$

where $k=\omega/c$ and $k_L=\omega/c_L$ are the wavenumbers associated with the uncoupled acoustic and longitudinal waves respectively. The equations (3) have non-trivial solutions if the determinant of the matrix is equal to zero. This condition leads to the following dispersion equation :

$$\left[-\frac{1-\nu^2}{E}\frac{T}{A}\lambda^2 - \frac{1}{a^2} + k_L{}^2\right]\left[k_L{}^2 - \lambda^2\right]\left[k^2 - \lambda^2\right] - \frac{\nu^2\lambda^2}{a^2}\left[k^2 - \lambda^2\right] - \frac{2a\rho_0}{h\rho}\frac{k_L{}^2}{a^2}\left[k_L{}^2 - \lambda^2\right] = 0. \qquad (4)$$

Dispersion equation *(4)* is a third-order polynomial equation of in λ^2, which may give six wavenumber roots $\pm\lambda_1, \pm\lambda_2, \pm\lambda_3$, corresponding to three axisymmetric waves propagating inward and outward along the *x* axis of the membrane tube. Note that the term $\frac{2a\rho_0}{h\rho}$ present in equation (4) is the fluid loading term. For numerical applications, equation (4) is solved by using the values for the parameters given in Table 1.

Two cases are studied : the conservative case, where any dissipation is ignored and the non-conservative case, where acoustical and mechanical dissipations are taken into consideration. In the first case the two wave speeds *c* and c_L are such that c^2 and $c_L{}^2$ are real numbers. In the second case, the dissipation phenomena imply that the celerities (and the wavenumbers) become complex, leading to both propagation and attenuation phenomena. In harmonic regime and at low frequency, the acoustical dissipation is mainly due to the thermoviscous phenomena localised at the wall boundaries. This dissipation is then modeled using the following complex wavenumber [29]:

$$k = \frac{\omega}{c} = \frac{\omega}{c_0} + \alpha \cdot (1 - j), \tag{5}$$

where $\alpha \approx 3 \cdot 10^{-5} \sqrt{f} / a$ (at 20°C), $c_0 = 343.37 ms^{-1}$, f being the frequency and a the radius of the tube, c being the complex wave speed. In addition, the mechanical dissipation is modeled using a complex Young's modulus, which then also renders the wave speed c_L complex.

The dispersion branches associated with the three wavenumbers λ, (roots of (4)) are presented in Section 2.3.4. These branches can be interpreted, first of all, by considering two simplified cases : the case where both static preload T and Poisson's ratio ν are assumed to be zero, and the case where only static preload T is set at zero.

2.3.2 Korteweg's hypothesis *(ν=0, T=0)*

Considering the case where *T=0* and *ν=0*, the roots of the dispersion equation (4) are the wavenumbers are given by :

$$\lambda = \pm \frac{\omega}{c_L} \quad \text{and} \quad \lambda = \pm \frac{\omega}{c_K}, \tag{6}$$

where

$$c_K = c \left[1 + \frac{2a\rho_0 c^2}{h\rho {c_L}^2 (1 - a^2 {k_L}^2)} \right]^{-1/2}. \tag{7}$$

Two waves propagate in the medium: a purely longitudinal wave in the membrane (wavenumber $k_L = \omega / c_L$) and a Korteweg's wave (wavenumber ω / c_K), the wave speed of which is denoted c_K. Numerical results are given in Figure 2 using the parameters from Table 1. The real parts of the complex speeds *Re(c_L), Re(c_K),* which are always positive (or null) are displayed in the positive half-plan. The imaginary parts *Im(c_L), Im(c_K)* are always negative (or null), and are displayed in the negative half-plan.

The longitudinal wave involves membrane displacement in the axial direction only *u* and is strictly uncoupled from bending displacement *w* and acoustic pressure *p* as should be the case

since the Poisson's ratio is zero. Korteweg's wave involves coupled oscillations between acoustic pressure p and bending membrane displacement w. In this case, no axial displacement is involved. This wave is highly dispersive. Three frequency ranges can be distinguished from expression (7).

In the range [0, f_a] where $f_a = c_L/(2\pi a)$ is the ring frequency of the membrane, the wave speed c_K is real and the propagating wave is subsonic ($c_K < c$, c being the speed of sound without any couplings). In this range, the wave speed c_K varies from

$$c_{K0} = \frac{c}{\left[1 + 2a\rho_0 c^2 / h\rho {c_L}^2\right]^{1/2}}$$

for $f = 0\ Hz$, to $c_K = 0$ for $f = f_a$. The low frequency limit c_{K0} is called Korteweg-Lamb wave speed [7] or Moes-Korteweg wave speed [20]. In the range $[\, f_a, f_a\sqrt{1 + 2a\rho_0 c^2/(h\rho {c_L}^2)}\,]$, wave speed c_K is a pure complex imaginary number (${c_K}^2 \le 0$) and the corresponding wave is evanescent. This range corresponds to a stop band. In the range $[\, f_a\sqrt{1 + 2a\rho_0 c^2/(h\rho {c_L}^2)}, +\infty[$, the wave speed is once again real. The corresponding propagating wave is supersonic ($c_K > c$) and varies from $c_K = \infty$ to $c_K = c$. Such a simple definition of ranges is possible because the dissipation has been ignored (Figure 2a). If it is taken into consideration, in the subsonic and supersonic ranges the complex wave speed c_K has a small imaginary part leading to wave attenuation. In the stop band, the real part of the wave speed c_K is not strictly equal to zero and corresponds to a highly damped propagating wave (Figure 2b). However, conclusions for the dispersion curves of the dissipative system remain qualitatively the same as for those using the conservative system.

2.3.3 Unstretched case (ν≠0, T=0)

Setting the static preload T to 0 in the dispersion equation (4) leads to

$$\lambda = \pm\frac{\omega}{c_1}, \lambda = \pm\frac{\omega}{c_2}, \tag{8}$$

where

$$\left(\frac{\omega}{c_1}\right)^2 = (-\beta + \sqrt{\Delta})/2 \quad \text{and} \quad \left(\frac{\omega}{c_2}\right)^2 = (-\beta - \sqrt{\Delta})/2, \tag{9}$$

with

$$\begin{aligned} \beta &= [(1/a^2 - {k_L}^2)({k}^2 + {k_L}^2) - \nu^2 k^2/a^2 + 2\rho_0 {k_L}^2/(ah\rho)]/[{k_L}^2 - (1-\nu^2)/a^2], \\ \Delta &= \beta^2 - 4\left[{k_L}^2 k^2 [{k_L}^2 - 1/a^2] - 2\rho_0 {k_L}^4/(ah\rho)\right]/[{k_L}^2 - (1-\nu^2)/a^2]. \end{aligned} \tag{10}$$

Two coupled waves propagate in the medium. At high frequencies it can be verified that the celerities c_1 and c_2 tend respectively towards c and c_L, indicating that the corresponding waves tend towards the plane wave in fluid and towards the longitudinal wave in the membrane, each wave being uncoupled from the other. The wave associated with $\lambda = \omega/c_1$ is close to Korteweg's wave, being slightly disturbed by the coupling between the longitudinal and flexural motion induced by Poisson's ratio. The wave associated with $\lambda = \omega/c_2$ is close to the longitudinal wave in the membrane.

2.3.4. General case (ν≠0, T≠0)

In the general case (ν≠0, T≠0), the three pairs of roots of the dispersion equation

$$\lambda = \pm\frac{\omega}{c_1},\ \lambda = \pm\frac{\omega}{c_2},\ \lambda = \pm\frac{\omega}{c_3}$$

can be numerically obtained and are presented in Figure 4 for the conservative case (a), and the dissipative case (b). The first two dispersion branches are close to the two obtained in the unstretched case ((T=0 , ν≠0). The third branch appears only when the membrane is subjected to tension. This coupled wave can be interpreted as a type of "string wave".

2.4. Acoustic input impedances

The wavenumbers derived in the previous section are used to calculate the acoustic input impedance for the fluid-filled membrane tube. Since the acoustic input impedance can be precisely measured, it permits a validation of the model. Computation of this acoustic impedance is performed in this section.

Six boundary conditions are associated to the problem: the membrane is assumed to be clamped at both ends. Subsequently, the mechanical boundary conditions at both $x=0$ and $x=L$ are : $u(0) = u(L) = w(0) = w(L) = 0$. A known harmonic velocity is imposed at one end of the tube. Subsequently, the acoustical boundary conditions at $x=0$ are $v(0)=v_0$, v being the acoustic particle velocity and v_0 being the imposed value of the velocity. The tube is assumed to be open at its other extremity $x=L$, which imposes the radiation impedance at this point (see below).

The acoustic pressure throughout the length of the tube can be written as the superposition of the 3 pairs of ingoing and outgoing waves:

$$p = A_1 e^{j\lambda_1 x} + B_1 e^{-j\lambda_1 x} + A_2 e^{j\lambda_2 x} + B_2 e^{-j\lambda_2 x} + A_3 e^{j\lambda_3 x} + B_3 e^{-j\lambda_3 x}. \tag{10}$$

The Euler equation gives a relationship between the acoustic pressure and the acoustic velocity:

$$j\omega\rho_0 v = -\frac{\partial p}{\partial x}. \tag{11}$$

The acoustic velocity can be written using equations (10) and (11) as follows:

$$v = -\left[\lambda_1\left(A_1 e^{j\lambda_1 x} - B_1 e^{-j\lambda_1 x}\right) + \lambda_2\left(A_2 e^{j\lambda_2 x} - B_2 e^{-j\lambda_2 x}\right) + \lambda_3\left(A_3 e^{j\lambda_3 x} - B_3 e^{-j\lambda_3 x}\right)\right] \Big/ \omega\rho_0 . \tag{12}$$

The input impedance Z is the ratio between the acoustic pressure and the acoustic velocity at $x=0$. Expressions (10) and (12) lead to the following expression

$$Z = \frac{p(x=0)}{v(x=0)} = \frac{A_1 + B_1 + A_2 + B_2 + A_3 + B_3}{\lambda_1\left(A_1 - B_1\right) + \lambda_2\left(A_2 - B_2\right) + \lambda_3\left(A_3 - B_3\right)} \omega\rho_0 . \tag{13}$$

The six unknowns are the amplitudes A_1, A_2, A_3, B_1, B_2 and B_3 which are determined from the boundary conditions. Five of them have already been described. The last is related to the open end extremity: at $x=L$, the acoustic impedance is set to :

$$Z(L) = \rho_0 c\left(0.25(\omega a/c)^2 - 0.7\, j\omega a/c\right). \tag{14}$$

Using equations (10) and (12), boundary conditions yield to a set of linear equations:

$$\begin{bmatrix} f_1(\lambda_1) & f_1(-\lambda_1) & f_1(\lambda_2) & f_1(-\lambda_2) & f_1(\lambda_3) & f_1(-\lambda_3) \\ f_2(\lambda_1) & f_2(-\lambda_1) & f_2(\lambda_2) & f_2(-\lambda_2) & f_2(\lambda_3) & f_2(-\lambda_3) \\ f_3(\lambda_1) & f_3(-\lambda_1) & f_3(\lambda_2) & f_3(-\lambda_2) & f_3(\lambda_3) & f_3(-\lambda_3) \\ f_4(\lambda_1) & f_4(-\lambda_1) & f_4(\lambda_2) & f_4(-\lambda_2) & f_4(\lambda_3) & f_4(-\lambda_3) \\ f_5(\lambda_1) & f_5(-\lambda_1) & f_5(\lambda_2) & f_5(-\lambda_2) & f_5(\lambda_3) & f_5(-\lambda_3) \\ f_6(\lambda_1) & f_6(-\lambda_1) & f_6(\lambda_2) & f_6(-\lambda_2) & f_6(\lambda_3) & f_6(-\lambda_3) \end{bmatrix} \begin{bmatrix} A_1 \\ B_1 \\ A_2 \\ B_2 \\ A_3 \\ B_3 \end{bmatrix} = \begin{bmatrix} v_\circ \\ 0 \\ 0 \\ 0 \\ 0 \\ 0 \end{bmatrix}, \tag{15}$$

where

$$\left.\begin{aligned} f_1(\lambda_i) &= -\lambda_i/(\omega\rho_0) \\ f_2(\lambda_i) &= e^{j\lambda_i L} \\ f_3(\lambda_i) &= \frac{\lambda_i^2 - k^2}{2\rho_0\omega^2/a} \\ f_4(\lambda_i) &= \frac{\lambda_1^2 - k^2}{2\rho_0\omega^2/a} e^{j\lambda_i L} \\ f_5(\lambda_i) &= \frac{jv\lambda_i}{2\rho_0\omega^2} \frac{k^2 - \lambda_i^2}{k_L^2 - \lambda_i^2} \\ f_6(\lambda_i) &= \frac{jv\lambda_i}{2\rho_0\omega^2} \frac{k^2 - \lambda_i^2}{k_L^2 - \lambda_i^2} e^{j\lambda_i L} \end{aligned}\right\} / i = \{1,2,3\}.$$

By solving equation (15), the six unknowns A_1, A_2, A_3, B_1, B_2, B_3 can be determined. As such, the acoustic input impedance of the membrane waveguide can be computed using (13). Normalised input impedances (dimensionless impedances $\overline{Z} = \frac{Z}{\rho_0 c_0}$) are plotted in Figure 5 by using the numerical values given in Table 1 for two tension values. Two simulated cases – with and without tension – are presented together, showing the slight influence of the tension on the calculated impedance. At high frequencies, the calculated input impedance is similar to that of a rigid tube. This indicates that the Korteweg's wave, the speed of which tends towards c_o at high frequencies (see Figure 2), is predominant. At low frequencies, several resonances can be observed. These appear to correspond to a wave speed less than c_o. In the medium frequency range, around 500 Hz, no resonance emerges. This can be explained by the fact that only evanescent waves exist in this stop band here (Figure 2). In the high frequency range, acoustic resonances tend to become harmonic and the impedance is similar to that of a rigid tube.

2.5. Equivalent wave speeds

Vibratory and acoustic fields of the coupled membrane are described as the superposition of three standing waves. The separation of the three waves is not an easy task. Consequently, a direct comparison between theoretical dispersion curves and experimental results also becomes difficult. In order to compare theoretical calculations with experimental results, an equivalent wave speed c_{eq} is defined. This equivalent wave speed may allow a partial comparison, by defining a kind of general speed of sound. It is computed from the input impedance as given below. The input impedance of a lossless rigid open tube is given by

$$Z_o = j\rho c \tan(kL). \tag{16}$$

For a vibrating tube whose input impedance is Z, the equivalent speed c_{eq} is defined by making an analogy with the case of the lossless rigid open tube. It corresponds to the value of wave speed for which the equation

$$Z = j\rho c \tan\left(\frac{\omega L}{c_{eq}}\right), \tag{17}$$

is satisfied. Definition (17) leads to the explicit expression

$$c_{eq} = \frac{\omega L}{(k\ L)_{eq}}, \tag{18}$$

with $(k\ L)_{eq} = \arctan\left(Z \big/ j\rho c\right) + n\pi$, n being an integer. In fact, an ambiguity exists since the *arctan* function provides a result between $-\pi/2$ and $\pi/2$ for its real part (Figure 6). To obtain the correct velocity for the rigid pipe, the integer n needs to be incremented after each phase jump (this is usually called “unwrapping”). In the present case, a difficulty arises due to the fact that the wavenumber is not a monotonous function of the frequency because of the stop band. Indeed, a frequency range exists for which the waves are evanescent. Therefore, the two frequency bands in which the waves are non-evanescent should be considered separately. The first band is from zero to the first cut-off frequency (close to f_a as shown in paragraph 2.3.2). The second band is from the second cut-off frequency (close to

$f_a\sqrt{1+2a\rho_0 c^2/(h\rho {c_L}^2)}$ as seen in paragraph 2.3.2) to infinite. For the first band, the initial value of n is zero. For the second band, the initial value n_0 at the beginning of the band is obtained using the fact that the equivalent speed tends towards the speed of sound when the frequency tends towards infinity (Figure 6).

The equivalent speed c_{eq} is then directly calculated from the correctly unwrapped function using equation (16). The results are displayed in Figure 7. In this figure, the wave speeds resulting from the dispersion curves (Figure 2b) are reprinted for reasons of comparison. The following conclusions can be drawn. At a high frequency (in the frequency range labelled C in Figure 7 and defined by $f > f_a\sqrt{1+2a\rho_0 c^2/(h\rho {c_L}^2)}$), c_{eq} is accurately superimposed on the one speed wave curve which tends towards $c_0 = 343.37 ms^{-1}$. This indicates that for the high frequency range, one of the three waves is predominant. In the low frequency range (frequency range A, defined by $f < f_a$) c_{eq} is not exactly superimposed on one or other of the speed wave curves. This suggests that the three waves might have a significant role to play regarding the impedance. However, c_{eq} is close to the Korteweg's speed, indicating that the Korteweg's wave is predominant within this frequency range. In the medium range B ($f_a < f < f_a\sqrt{1+2a\rho_0 c^2/(h\rho {c_L}^2)}$), no clear conclusion can be drawn : the equivalent speed differs greatly from the speeds of the three natural waves in the system. This is not surprising in this case as the evanescent behaviour is predominant. We conclude that the speed of the Korteweg's wave within the ranges A and C may be determined approximately by computing the equivalent speed.

3. Measurements and discussion

A partial experimental validation is proposed in this section : the equivalent speed is extracted from the measured acoustic input impedance of a rubber membrane. The results are compared to the theoretical model given in the previous section.

3.1. Experimental set-up

The input impedance is measured using the impedance sensor described in [30]. This sensor uses a half-inch electrostatic microphone cartridge as a volume velocity source and an electret microphone as a pressure sensor. The use of a microphone cartridge has been chosen as a

source because its frequency response is flat and its mechanical impedance is relatively high. The limitation of this source is that, for a given input signal amplitude, the volume velocity is proportional to the frequency and tends towards zero with frequency. The microphone cartridge and the electret microphone are fixed onto a stiff metal plane which constitutes the reference plane for the measurements. The measurements are carried out in an anechoic chamber with a dual-phase lock-in amplifier including a sine source used for both excitation and demodulation. It is calibrated with the procedures for input and the transfer impedance measurements as described in [30], [31]. The rubber tube is fixed to the impedance sensor using a specially designed set-up which allows for any variation in tube tension (Figure 8). For verification purposes, prior to the measurement of the rubber tube, the input impedance of a rigid aluminium tube of approximately the same dimensions is measured and compared with a theoretical model. When considering the uncertainties in the model (especially in the radiation impedance) the measurement is considered to be in accordance with the model, thus validating the measurement procedure of the acoustic input impedance.

3.2. Preliminary observations

In addition to the input impedance measurements, the radial velocity of the membrane is scanned using a laser vibrometer which can be moved along its axis. Measurements are carried out on the rubber tube, the characteristics of which are given in Table 1. Typical results are given in Figure 9. In such cases, no tension has been applied to the membrane and its end is closed. The configuration is thus slightly different to the one previously described; however, the wave types existing in the coupled system remain the same. The aim of these preliminary vibration measurements is to clearly demonstrate the existence of several waves within the coupled system : the Korteweg's wave and the longitudinal/flexural wave. The third wave (termed the 'string wave') does not exist since no tension has been applied.

The vibration level of the membrane is plotted in Figure 9d as a function of the axial coordinate x and the frequency. The three ranges A (subsonic range), B (evanescent range) , C (supersonic range) described in paragraph 2.3.2 are clearly visible on the map. Three vibration profiles (9a-9c) are extracted from Figure 9d and correspond to frequencies selected in the ranges A, B, and C. In Figure 9d, the horizontal lines are plotted at the selected frequencies (490Hz, 690Hz and 1190Hz). In the frequency range ranges A and C, the vibration profiles presented in Figures 9a, 9c (and also visible on map 9d) show that the field is composed of two waves : a short and a long wave length, corresponding to wave speeds c_1 and c_2

respectively (see relations (8) and (9)), can be identified. In this case, the vibratory field is composed of two standing waves whose nodes and crest are visible. The attenuation of the wave associated with c_1 is visible due to the fact that its contribution is only significant in the vicinity of the ends $x=0$ and $x=0.5m$. In range B, no standing waves are visible because the evanescent contribution is dominant here. From this preliminary investigation it should be concluded that the two waves (the Korteweg's wave and the coupled longitudinal/bending wave) can be observed at the experimental stage and lead to a standing wave system. An initial comparison between these experimental results and the theory previously described should be possible. However, a theory/experiment comparison based on the input acoustic impedance has been chosen in preference.

3.3. Measured input impedances for an unstretched membrane

The measured input impedance for the rubber tube without static preload is displayed in Figure (10). As already pointed out in Section 2.3.2 which deals with theory, three frequency ranges can be observed on the curve. For the higher frequency range (the range labelled C and defined by f >1000Hz), regularly spaced impedance peaks can be seen and the input impedance tends towards that of a rigid tube. In the lower frequency range, (the range labelled A corresponding to f < 600Hz), two resonances can be identified. The frequency shift between these two resonances indicates that the corresponding speed wave is lower than c_o the acoustic wave speed in air. In the medium frequency range (range B), between 600 and 1000 Hz, only one resonance of low Q-factor is present. This confirms the theoretical results shown in Figure 5 : that, in this range, the fluid-membrane coupling is important, and the evanescent wave phenomenon is predominant.

In order to compare theoretical and experimental results, the Young's modulus of the rubber ($E= E'+jE''$) has been measured versus frequency. Results for this auxiliary measurement are presented in appendix B. Theoretical input impedance is computed from (13) using the measured values of E' and E'' , and taking into consideration the radiation impedance condition (14). A very close agreement between the theoretical and measured input impedances is observed.

3.3. Estimated equivalent wave speed for stretched membranes

In this section the influence of the tension of the membrane is examined: the input impedance has been measured for three different static preloads : 0 N (which is the case presented in Figure 10), 24 N and 40 N. These correspond respectively to an extension of the rubber tube of 0 m, 0.03 m (that is 6% of the length) and 0.06 m (11%). The corresponding $(kL)_{eq}$ is calculated (Figure 11a) as explained in Section 2.4. These should be compared with the theoretical results displayed in Figure 6. As previously explained, the functions do not increase monotically as a function of the frequency ("unwrapped" arctangent). After having unwrapped the functions, the $(kL)_{eq}$ variables can be obtained (Figure 11b), and, subsequently, the equivalent wave speeds c_{eq} can be obtained using equation (16). These are displayed in Figure 12 to facilitate a comparison with the theoretical results displayed in Figure 7.

For the lower and higher frequency range, the effect of the tension is clearly visible in $(kL)_{eq}$. Conversely, the effect disappears when the equivalent wave speed is calculated. This indicates that the effect of tension is essentially to increase the length of the tube. On the other hand, for the medium frequency range, the effect of tension is not visible in $(kL)_{eq}$, signifying that the tension has no significant influence on the mechanical characteristics of the tube. Naturally, in the medium frequency range, an effect on the equivalent wave speed can be observed. However, as the waves in this range are evanescent, the length of the pipe does not influence the impedance. In conclusion, it can be said that for the tension under consideration, which corresponds to an extension of the length of the tube by as much as 10%, tension does not significantly influence the mechanical properties of the tube. A much higher tension is necessary in order to observe a significant effect.

4. Conclusion

Wave propagation inside a stretched elastic cylindrical tube is studied under plane wave approximation. Two models have been used. The first one is known as the Korteweg's model in which the walls are characterised by their locally reacting impedance. Using this model, two propagating waves can be identified : one mainly propagates within the fluid and is called the Korteweg's wave, the second is the longitudinal wave which propagates in the structure. The Korteweg's wave exhibits different behavior according to the frequency. Three frequency ranges are emphasized. For the lower frequency range, the wave is subsonic. For the medium

range the wave is evanescent and for the higher frequency range the wave is supersonic and the wave speed tends towards the speed of sound in air. A second more sophisticated model has been derived, which leads to three propagating waves: two of which are very close to those previously described. The third one is induced by the tension of the tube and corresponds to a string wave. The acoustic input impedance of the tube is computed in order to compare the results with those resulting from the Korteweg's model and also with those provided by the experiments. An equivalent wave speed has been defined from the input impedance under the assumption that a unique wave is propagating, and using the analogy with the rigid tube. For the three waves model, the results are similar to those obtained using the Korteweg's model which demonstrates that this model is a fitting approximation for the calculation of the acoustic inner field. Indeed, if three different waves contribute to the field, one wave, which can be assimilated to the Korteweg's wave dominates and, hence, the contribution of the other waves might be neglected as in the case of the rubber tube being investigated. This result is in accordance with [22], [23].

Theoretical results are compared with the measured input impedances of a stretched rubber tube membrane. The displayed measured input impedances exhibit the same three frequency ranges as described in the theoretical results. Moreover, the equivalent wave speed has been derived from the measured input impedances, showing a good agreement between the theoretical and experimental equivalent celerities. This shows that the inner acoustic pressure's field is mainly dominated by the Korteweg's wave for which propagation is subsonic within the low frequency range and supersonic in the high frequency range tending towards the speed of sound in air.

Acknowledgements

The authors wish to thank B. Jullin for his participation in this work .

APPENDIX A : MOTION EQUATIONS OF THE STRETCHED MEMBRANE

The membrane operator can be obtained from the Donnell's shell operator as given in reference text books [1], [33], assuming that the thickness parameter $\frac{h^2}{12a^2}$ is set at zero. This operator can be modified in order to take into consideration the static preload effect. In this appendix, we derive the useful relationships leading to the motion equations (1), assuming the membrane hypothesis and the axisymmetry of the vibratory field.

The forces applied to a membrane element of size (dx, $ad\theta$) are given Figure A1. The normal force in the axial direction and in the circumferential direction are N_x and N_θ; the transverse shear force is Q_x. The acoustic pressure acting on the membrane element is labelled p. Projections for the motion equations in the axial and radial directions are written as

$$\rho h \frac{\partial^2 u}{\partial t^2} = \frac{\partial N_x}{\partial x}, \tag{A1}$$

$$\rho h \frac{\partial^2 w}{\partial t^2} = -\frac{N_\theta}{a} - \frac{\partial Q_x}{\partial x} + p, \tag{A2}$$

The normal stresses in the axial and circumferential directions σ_{xx} and $\sigma_{\theta\theta}$ and the shear stress $\sigma_{x\theta}$ are related to strains ε_{xx}, ε_{xx}, ε_{xx} by

$$\sigma_{xx} = \frac{E}{1-\nu^2}(\varepsilon_{xx} + \nu\varepsilon_{\theta\theta}), \qquad \sigma_{\theta\theta} = \frac{E}{1-\nu^2}(\varepsilon_{\theta\theta} + \nu\varepsilon_{xx}), \qquad \sigma_{x\theta} = \frac{E}{1+\nu}\varepsilon_{x\theta}. \tag{A3}$$

The relationships between stresses and displacements are given by

$$\varepsilon_{xx} = \frac{\partial u}{\partial x}, \qquad \varepsilon_{\theta\theta} = \frac{w}{a}, \qquad \varepsilon_{x\theta} = 0. \tag{A4}$$

In order to take into account the static preload, we assume that static stresses in the membrane are $\sigma_{xx}{}^s = \frac{T}{A}$, and $\sigma_{\theta\theta}{}^s = \sigma_{x\theta}{}^s = 0$. This hypothesis is valid for points which are sufficiently distant from the boundary conditions. From (A3), the static strains are obtained as $\varepsilon^s{}_{xx} = \frac{T}{AE}$, $\varepsilon^s{}_{\theta\theta} = \frac{-\nu T}{EA}$, $\varepsilon^s{}_{x\theta} = 0$ and from relation (A4), the static displacements are found in the form of $u^s = \frac{T}{AE}x$ and $w^s = \frac{-\nu T}{EA}$.

Since the kinematic membrane hypothesis is assumed, displacements u and w are supposed to be independent of the radial co-ordinate and are written as the sum of static terms (u_s, w_s) and dynamic terms (u^0, w^0) :

$$u = u^s + u^0, \qquad w = w^s + w^0. \tag{A5}$$

Taking the displacements fields (A5) as a starting point, in which the static displacements are known, the strains are obtained from (A4), the stresses from (A3), and by integrating the stresses over the membrane thickness, the resulting forces are acquired

$$N_x = \int_{-h/2}^{h/2} \sigma_{xx} dz = \frac{Th}{A} + \frac{Eh}{(1-\nu^2)}\left[\frac{\partial u^0}{\partial x} + \nu \frac{w^0}{a}\right], \tag{A6}$$

$$N_\theta = \int_{-h/2}^{h/2} \sigma_{\theta\theta} dz = \frac{Eh}{(1-\nu^2)}\left[\frac{w^0}{a} + \nu \frac{\partial u^0}{\partial x}\right], \tag{A7}$$

$$Q_x = -N_x \frac{\partial w}{\partial x} = -\frac{Th}{A}\frac{\partial w^0}{\partial x}. \tag{A8}$$

Inserting (A6), (A7) and (A8) into the motion equations (A1) and (A2) provides the final form for the motion equations (1).

APPENDIX B : MEASUREMENT OF THE COMPLEX YOUNG'S MODULUS VERSUS FREQUENCY

The mechanical properties of rubber depend on temperature and frequency. The ageing of the material can also modify the values of its Young's modulus. Experimental determination of the complex Young's modulus E of the rubber constituting the membrane is briefly described in this appendix. The value of E is used for computing the theoretical input impedance.

A Dynamic Mechanical Analyzer (TA Instruments 2980) has been used. The measurement method is based on measurement of the transfer function between extensional strain and stress applied to a sample. The complex Young's modulus $E = E' + iE''$ is deduced from this transfer function. Measurements are performed using a stepped sine excitation in a reduced frequency range (0.1-50Hz) for 9 temperature controlled environments between –30°C and 40°C. The time-temperature superposition method is used to extend the frequency range [32] : for polymeric viscoelastic materials, decreasing temperature or increasing frequency. The curves *E'* and *E''* versus frequency obtained in the reduced frequency range at different temperatures are shifted according to frequency in such a way that they are superimposed at a given temperature. Results are given in figure B1 at 20°C. A linear fit in the log-log plane is plotted, showing that frequency dependence of *E'* and *E''* are power laws. Uncertainties are estimated to ±15% and the corresponding limit values for *E'* and *E''* are presented in the same graph. For the rubber under consideration, the fit of the experimental data leads to the empirical expressions

$$E' = 10^{6.336} f^{0.054} \text{ (Pa)} \qquad \text{(B1)}$$

$$E'' = 10^{5.363} f^{0.089} \text{ (Pa).} \qquad \text{(B2)}$$

Typical values for *f=1000Hz* correspond to $E=E_0(1+j\delta)$ MPa, with E_0=3.16MPa and δ=0.13.

REFERENCES

1. A. W. Leissa, *Vibrations of Shells*. Washington, DC: NASA, 1973.
2. C. R. Fuller and F. J. Fahy, Characteristics of wave propagation and energy distributions in cylindrical elastic shells filled with fluid. *Journal of Sound and Vibration* **81**(4), 1982, 501-518.
3. V.N. Merkulov, V.Y Prikhod'ko, V. V. Tyutekin, Excitation and propagation of normal modes in a thin cylindrical elastic shell filled with fluid. Normal modes in a thin cylindrical elastic shell filled with fluid and driven by forces specified in its surfaces *Soviet Physical Acoustics*, 24 (5), 1978, 51-54.
4. K. Trdak, Intensité vibratoire et acoustique dans les tuyaux, *PhD thesis*, Université Technologique de Compiègne, 1995 (*in French*).
5. R. Kumar, Dispersion of axially symmetric waves in empty and fluid-filled cylindrical shells, *Acustica* **27,** 1972, 317-329.
6. F. Gautier, N. Tahani, Existence of two longitudinal guided waves in a fluid-filled cylindrical duct with vibrating walls, *Inter-Noise Congress Proceedings*, 1996.
7. M. Junger, D. Feit, Sound structures and their interactions, MIT Cambridge, MA, 2nd ed., 1986.
8. J. Lighthill, Waves in fluids, Cambridge University Press, 2001.
9. P.M. Morse, K.U. Ingard, Theoretical acoustics, Princeton University Press, 1986.
10. H. Lamb, On the velocity of sound in a tube, as affected by the elasticity of the walls, *Memoirs and proceedings. ManchesterLiterary and Philosophical Society*, vol. 42 n°9, p. 1-16, 1898.
11. H. Levine, *Unidirectional wave motions*, North Holland Publishing Company, Amsterdam, New York, Oxford, 1978.
12. J.J. Fredberg, M. E. B. Wohl, G. M. Glass, H. I. Dorkin, Airway Area by Acoustic Reflections measured at the mouth, *Journal of Applied Physiology*, **48 (5)**, 1980, 749-758.
13. M.M. Sondhi, Model for wave propagation in a lossy vocal tract, *Journal of the Acoustical Society of America*, **55**(5), 1974, 1070-1075.
14. J. J. Fredberg, Acoustic determinants of respiratory system properties, *Annals of Biomedical Engineering*, **9**, 1981, 463-473.
15. Caliope, La parole et son traitement automatique, Collection technique et Scientifique des Télécommunications, Masson Editor, 1989 *(in French*).

16. S.I. Rubinow, J. B. Keller, Wave propagation in a viscoelastic tube containing a viscous fluid, *Journal of Fluid Mechanics*, Vol 8, part 1, 1978, 181-203.
17. F. Gautier, N. Tahani, Vibroacoustic behavior of a simplified musical wind instrument, *Journal of Sound and Vibration*, **213**, 1998, 107-125.
18. R. Pico, F. Gautier, J. Redondo, Acoustic input impedance of a vibrating cylindrical tube, *Submitted for publication to the Journal of Sound and Vibration, 2004.*
19. J. Backus, T.C. Hundley, Wall vibration in flue organ pipes and their effect on tone, Journal of the Acoustical Society of America, 39(5), 936-945, 1966.
20. R.W. Guelke, A.E. Bunn, Transmission line theory applied to sound wave propagation in tubes with compliant walls, *Acustica* **48**, 1981, 101-106.
21. T. Kamakura, Y. Kumamoto, Waveform distortions of finite amplitude acoustic wave in an elastic tube, *Frontiers of non linear acoustics: proceedings of the 12th ISNA*, edited by M. F. Hamilton and D. T. Blackstock, Elsevier Science Publishers Ltd, London, 1990, 333-338
22. V. Martin, Couplage fluide /structure : dispersion des ondes fluides guidées, *C. R. Acad. Sci. Paris*, **306**(2), 1988, 1-4 (in French).
23. V. Martin, Perturbation of fluid-guided waves induced by bending plates, *Journal of Sound and Vibration*, **144**(2), 1991, 331-353.
24. A. Wang, R.J. Pinnington, Investigation of the dynamic properties of the liquid filled pipework systems, *Proceeddings of the Institute of Acoustics*, vol.15 Part 3, 1993.
25. B.V. Chapnik, I. G. Currie, The effect of finite length flexible segments on acoustic wave propagation in piping systems, *Internoise Congress Proceedings*, Liverpool, U.K., 1996 , 1011-1014.
26. R. J. Pinnington, The axisymmetric wave transmission properties of pressurized flexible tubes, *Journal of Sound and Vibration*, **204** (2) 1997, 271-289.
27. R.J. Pinnington, Axisymmetric wave transfer functions of flexible tubes, *Journal of Sound and Vibration*, **204** (2), 1997, 291-310.
28. F. Fahy, Sound and Structural Vibration, Academic Press, 1985.
29. R. Caussé, J. Kergomard, X. Lurton, Input impedance of brass musical instruments – Comparison between experiment and numerical models. *Journal of the Acoustical Society of America,* **75** (1984), 241-254.
30. J.P. Dalmont, A. M. Brunneau, Acoustic impedance measurements: plane-wave mode and first helical mode contributions, *Journal of Acoustical Society of America* **91** (5), 1992, 3026-3033.

31. J.P. Dalmont, Acoustic impedance measurements Part II: a new calibration method, *Journal of Sound Vibration* **243** (3), 2001, 441-459.
32. J.D. Ferry, *Viscoelastic properties of polymers, J*ohn Willey, New York, 1961.
33. W. Flugge, Stresses in shells, Springer Verlag, 2nd Edition, 1973.

LIST OF FIGURES

Figure 9 : (d) Vibration level on a fluid-filled rubber membrane excited by a harmonic source at x=0m. The end of the tube (x=0.5m) is closed. The level (arbitrary unit) is depicted as a function of the axial co-ordinate x (m) and the frequency f (Hz), (a) the vibration profile of the membrane for f=490 Hz (subsonic range A). (b) the vibration profile of the membrane for f=690 Hz (evanescent range B). (c) the vibration profile of the membrane for f=1190 Hz (supersonic range C).

Figure 10 : Magnitude and phase of a measured (a) and theoretical (b) acoustic input impedance as a function of frequency in Hz.

Figure 11 : Not unwrapped (a) and unwrapped (b) variables $(kL)_{eq}$ associated with 3 measured input impedances.

Figure 12 : Equivalent wave speeds from the measured impedances corresponding to T=0N, T=20N, T=50N (thin lines) and celerities computed from equation dispersion dispersion (14), using measured values of E given in appendix B (thick lines).

Figure 13 : Forces applied to a membrane element

Figure 14 : Measurement of the real part E’ and imaginary part E’’ of the Young’s modulus E versus frequency.

Geometry	**Characteristics of the material (rubber type)**
Inner radius: a=0.015m Thickness: $h=0.0018m$ Length: $L=0.525m$	Density: $\rho = 921\ kgm^{-3}$ Young's modulus: $E=E_0(1+j\delta)$ $E_0=1.2\ \ 10^{6}\ Pa$, $\delta= 0.2$ Poisson's ratio : $\nu=0.5$

Table 1: Characteristics of the studied membrane

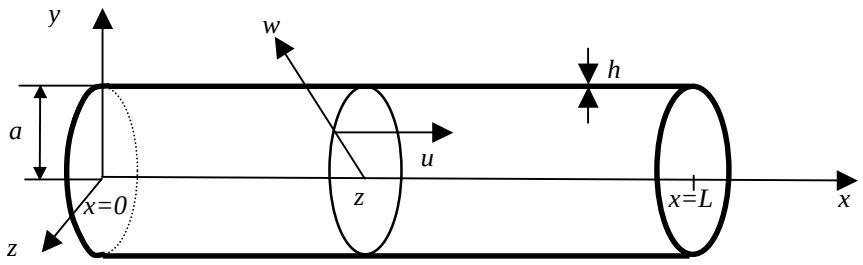

Figure 1 : co-ordinates and displacement sign convention for the vibrating cylindrical membrane .

(a) (b)

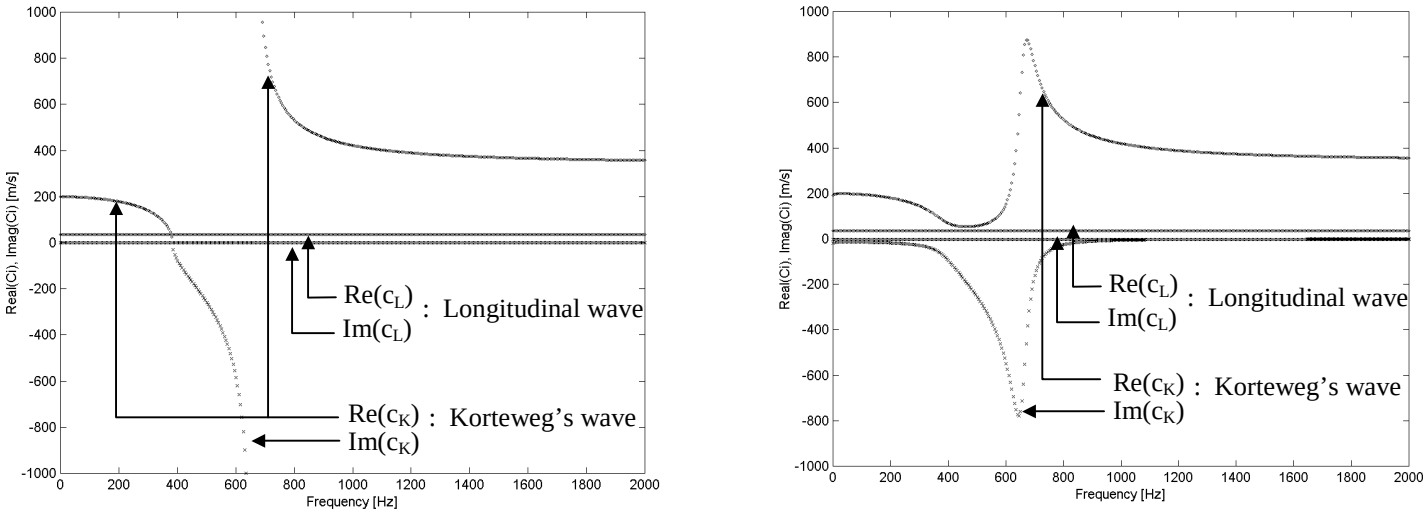

Figure 2 : Dispersion curves for the fluid-filled membrane assuming ν=0 and T=0, other parameters being given in table 1. Conservative case (a) corresponding to $E=E_0$ and dissipative case (b) corresponding to $E=E_0(1+j\delta)$. Real part (always positive) and imaginary part (always negative) of the complex wave speeds c_L and c_K in m/s are plotted versus frequency in Hz.

(a) (b)

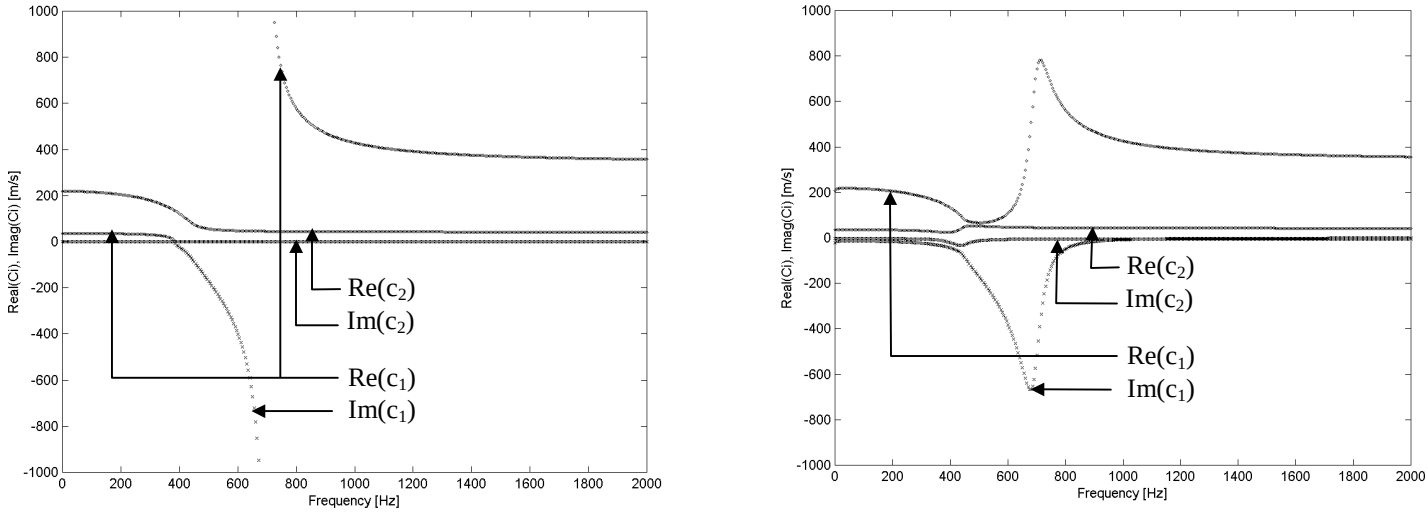

Figure 3 : Dispersion curves for the fluid-filled membrane in the unstretched case T=0 , $\nu \neq 0$, other parameters being given in table 1 . Conservative case (a) corresponding to $E=E_0$ and dissipative case (b) corresponding to $E=E_0(1+j\delta)$. Real part (always positive) and imaginary part (always negative) of the complex wave speeds c_1 and c_2 in m/s versus frequency in Hz.

(a) Conservative case (b) Dissipative case

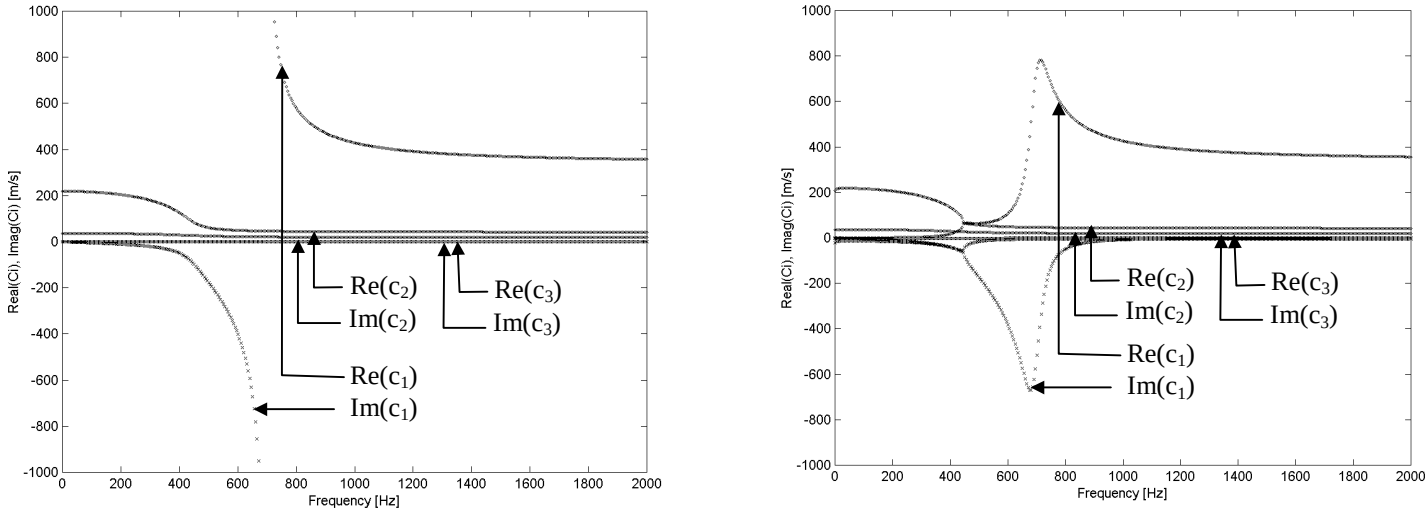

Figure 4 : Dispersion curves Dispersion curves for a stretched fluid-filled membrane T=50N, ν=0.5, other parameters being given in table 1 . Conservative case (a) corresponding to $E=E_0$ and dissipative case (b) corresponding to $E=E_0(1+j\delta)$. Real part (always positive) and imaginary part (always negative) of the complex wave speeds c_1, c_2, and c_3 in m/s versus frequency in Hz.

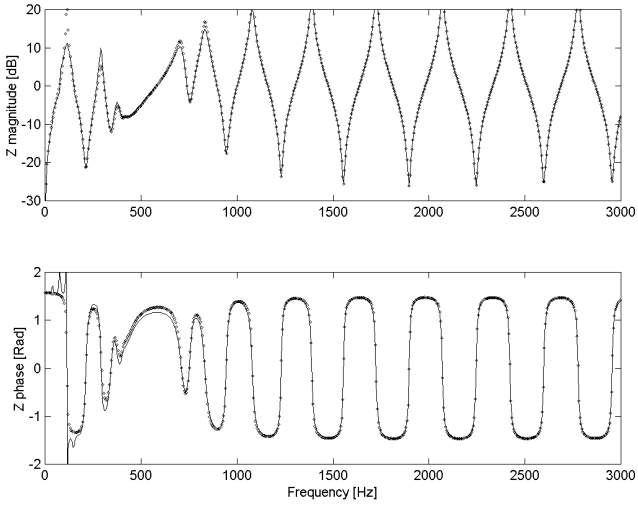

Figure 5 : Magnitude and phase of the specific acoustic input impedance of the vibrating membrane as a function of frequency. Case of a membrane without tension (thin line) and stretched with a tension T=50 N (dotted line) .

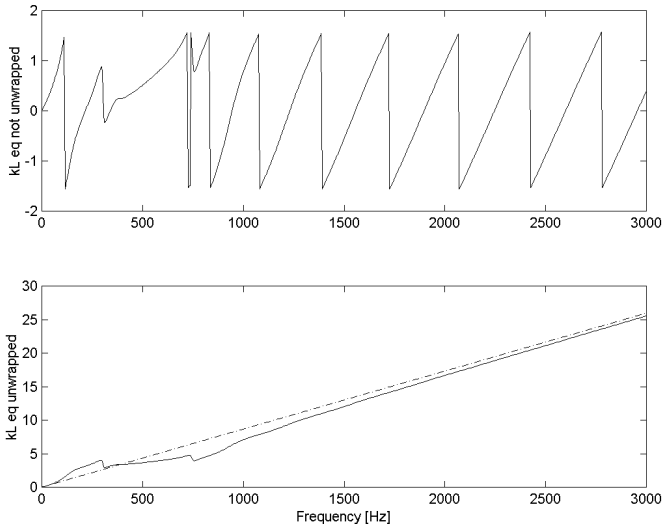

Figure 6 : Not unwrapped (a) and unwrapped (b) values of variable $(kL)_{eq}$ defined by relation (17), versus frequency for the vibrating tube defined by table 1. In figure (b), the dotted line indicates variable kL for the theoretical input impedance of the rigid tube.

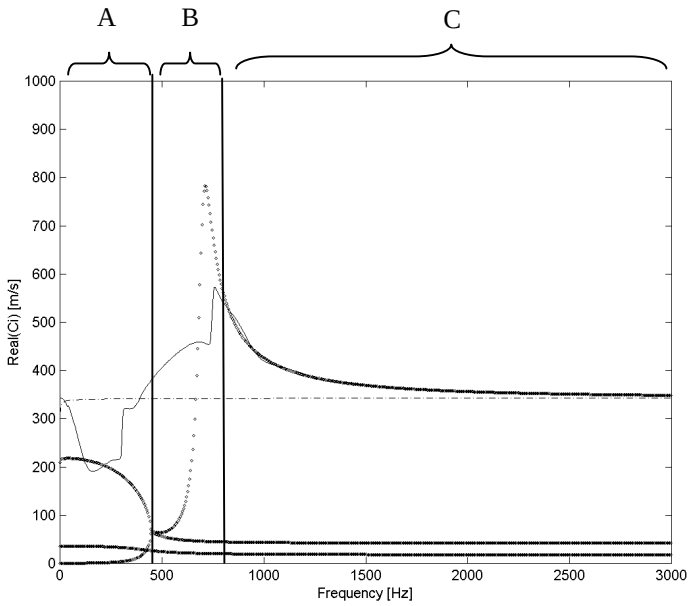

Figure 7 : Equivalent wave speed computed from simulated acoustic impedance for the stretched membrane described in table 1 (thin line). For reasons of comparison, the real part of the wave speeds computed from dispersion equation (4) is plotted with thick dots.

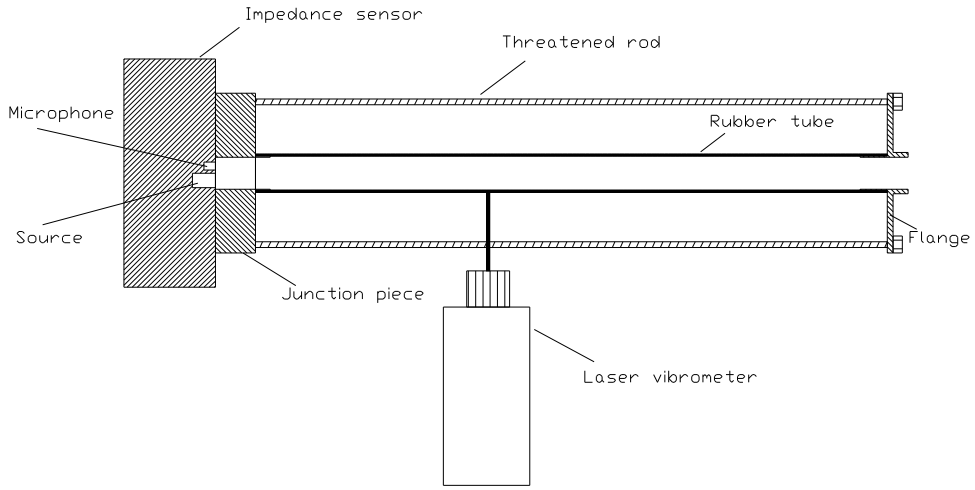

Figure 8 : Experimental set-up

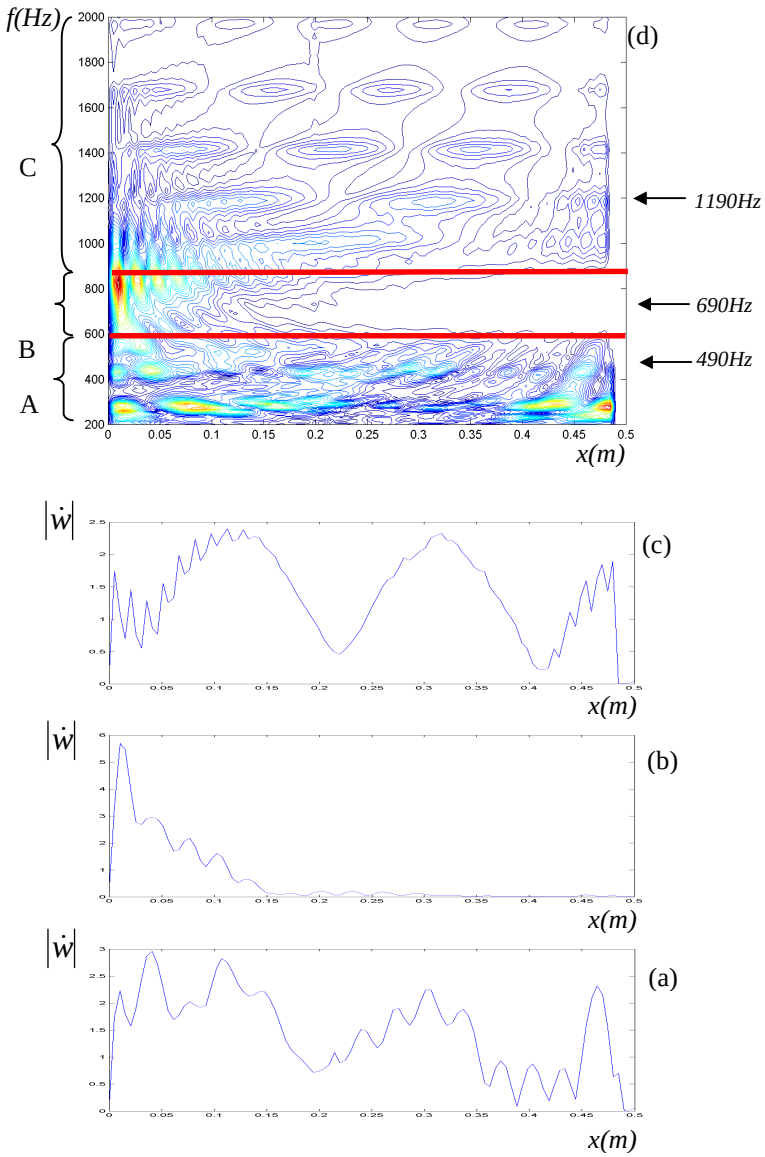

Figure 9 : (d) Vibration level on a fluid-filled rubber membrane excited by a harmonic source at *x=0m*. The end of the tube (*x=0.525m*) is closed. The level is depicted as a function of the axial co-ordinate *x (m)* and the frequency *f (Hz)* using an arbitrary unit. The red lines indicate the limits of the subsonic frequency ranges A, evanescent range B, supersonic range C. The vibration profile of the membrane $\dot{w}(x)$ along the axis is plotted in figure (a) for f=490 Hz (range A), in figure (b) for f=690 Hz (range B), in figure (c) for f=1190 Hz (range C).

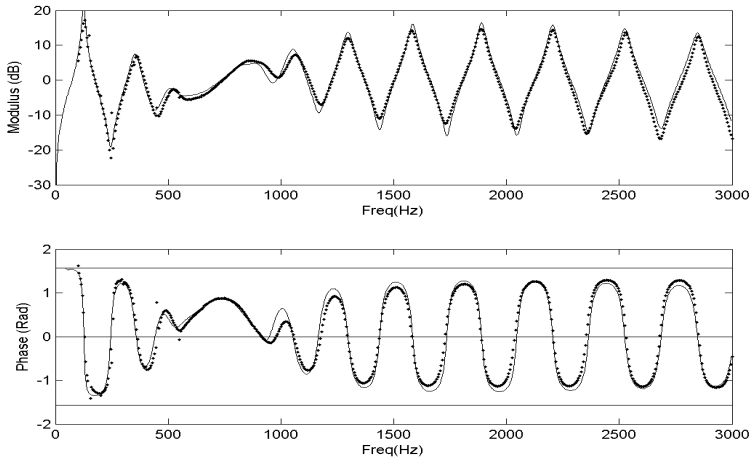

Figure 10 : Magnitude (a) and phase (b) of the measured (dotted line) and theoretical (continuous line) acoustic input impedance as a function of frequency in Hz. Characteristics of the membrane are given in table 1.

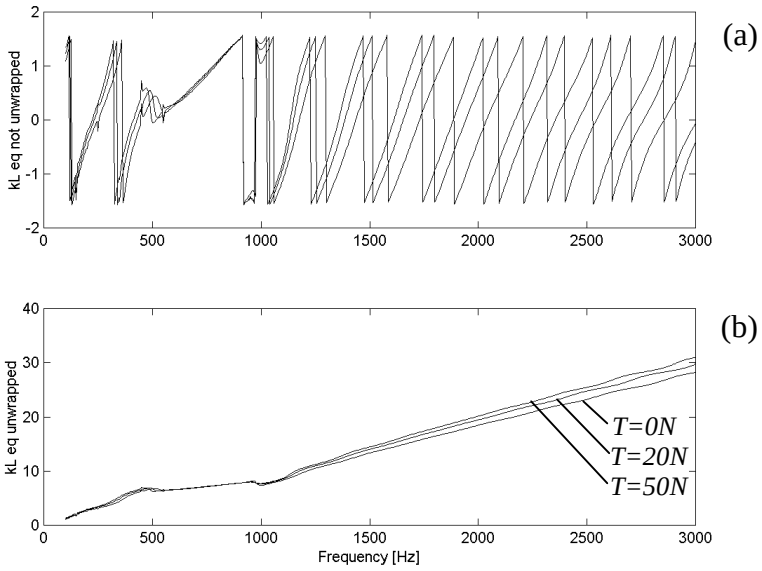

Figure 11 : Not unwrapped (a) and unwrapped (b) values of variable $(kL)_{eq}$ defined by relation (17) versus frequency. This variable is computed from the 3 measured input impedances obtained for tension T= 0N, T=20N and T=50N.

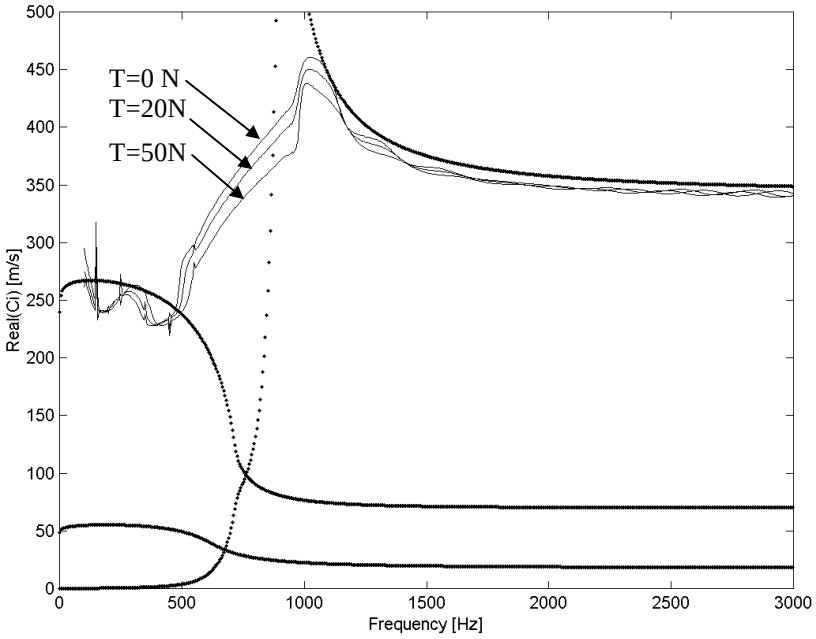

Figure 12 : Equivalent wave speeds computed from the measured impedances corresponding to tensions T=0N, T=20N, T=50N (thin lines) and computed from dispersion equation (14), using measured values of E given in appendix B (thick lines).

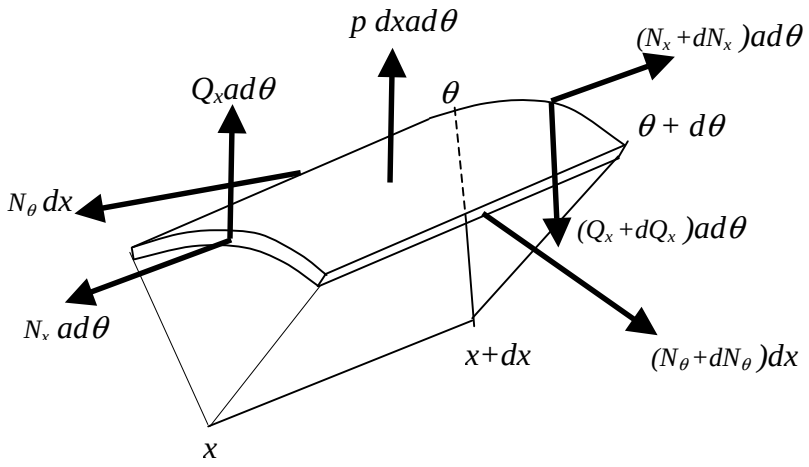

Figure 13 : Forces applied to a membrane element.

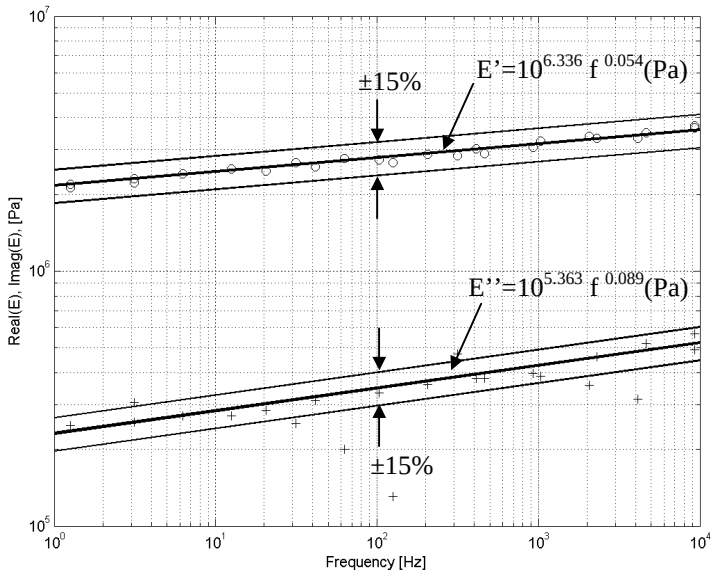

Figure 14 : Measurement of the real part E' and imaginary part E'' of the Young's modulus E versus frequency.